# Chapter 26
# Description and Preliminary Test Results of a Six Degrees of Freedom Rigid Wing Pumping System

Richard Ruiterkamp and Sören Sieberling

**Abstract** Ampyx Power develops a pumping kite system with a rigid aircraft that is attached to the tether by a single attachment point. This unbridled configuration allows three degrees of freedom (DOF) for the aircraft attitude and three for the position. The total system can be described by these 6 DOF. Operating the pumping kite system requires a novel view on conventional flight control. A tether based reference frame is introduced that in effect decouples the longitudinal and lateral motion which can then be designed independently allowing the highly dynamic motion of the glider to be controlled through simple control schemes. Furthermore the longitudinal motion is constrained through the tether of which the tangential velocity is controlled by the generator providing an additional control input besides the elevator to control longitudinal motion. Flight tests demonstrate that using the tether based flight control system reasonably simple and commonly used control methods provide satisfactory flight performance. This paper gives an overview of the system components and control strategy and gives a brief overview of preliminary flight tests and performance.

## 26.1 Introduction

The PowerPlane concept uses a standard glider aircraft that can roll, pitch and yaw by means of deflecting ailerons, elevator and rudder, respectively to change the attitude and flight path [2, 3]. The aircraft can also deploy flaps to increase lift and drag either to increase the maximum $C_L$, or when used together with the ailerons (flaps down, ailerons up) in a "crow" configuration to increase drag. Collectively these control surfaces are used to track a waypoint pattern based on the system state. This

Richard Ruiterkamp (✉) · Sören Sieberling
Ampyx Power B.V., Lulofsstraat 55 - 13, 2521AL Den Haag, The Netherlands, e-mail: r.ruiterkamp@ampyxpower.com

means that a different waypoint pattern is tracked for different parts of the control loop.

The aim of the complete control loop is to launch the aircraft, while attached to the tether, and insert it into the power production loop. During the power production loop, the tether is extracted from the drum of the ground winch until a preset maximum tether length is reached. After the maximum tether length is reached, the aircraft pitches down and flies a waypoint track that is directed towards the winch, while the winch is reeling in at full speed. When the minimum tether length is reached the aircraft transitions back into the power production pattern and the cycle is repeated.

This paper gives some insights in the PowerPlane system specifications and dimensions of the current prototype in Sect. 26.2. The flight control system of the PowerPlane is split into longitudinal and lateral control described in Sect. 26.3. In Sect. 26.4 some results from test flights are presented, followed by the conclusions in Sect. 26.5.

## 26.2 Overview of the PowerPlane system

The PowerPlane aircraft has a wingspan of 5.5 m and a wing surface area of 3 $m^2$. The wing has an aspect ratio of 10 and the total aircraft weight is 28 kg. Figure 26.1 shows the planform of the aircraft.

The ground station is a moving drum configuration that prevents the spooling mechanism from acting against the tether force. The current generator is of the direct drive type that does not require a gear-train. The generator is 98 % efficient and is directly connected to the main power grid through inverters in an AC-DC-AC configuration. The total electrical efficiency of the current system is rather poor at around 50 % and the focus of improvement.

Although the aircraft defines the magnitude of the lift, the tether dominates the drag and the lift to drag ratio of the system, see Fig. 26.2. For a free flying glider the lift to drag ratio provides a means to compare glider performance between different wing shapes and sizes in terms of the range and efficiency. For a tethered glider the system lift to drag ratio is however not independent of dimension and system lift to drag ratios of differently sized systems should not be compared without corrections.

The scaling dependency of the system lift to drag ratio is caused by the tether dimensioning. When expressing the scaling of the glider in terms of wing surface, twice as much wing surface results in twice as much lift and drag, hence tension. When the tension doubles, the tether cross-sectional area doubles. Since the system lift to drag ratio does not depend on tether cross section but on tether diameter, the effective tether drag coefficient will grow with the square root of the tether cross section, hence proportional to the square root of the wing surface. Therefore, the relative contribution of the tether drag becomes smaller (see Fig. 26.3). Note how-

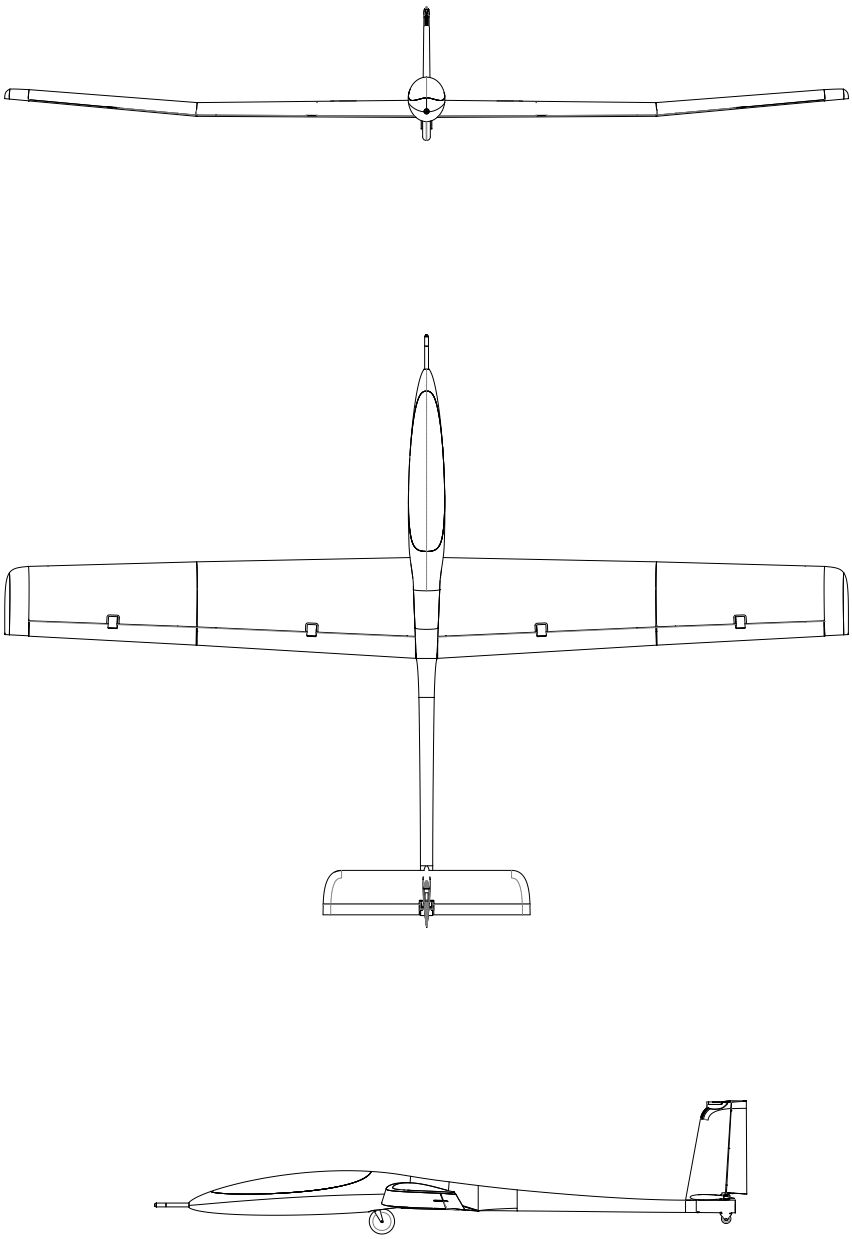

**Fig. 26.1** Planform of the PowerPlane nr. 6 with a wing span of 5.5 m and a wing surface area of 3 $m^2$

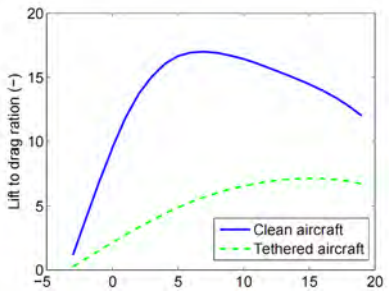


**Fig. 26.2** The lift to drag ratio of a clean free flying glider vs angle of attack compared to the lift to drag ratio of a tethered glider with a fixed tether length of 400 m vs. angle of attack.

ever that for larger wing spans it is likely that the tether length should increase as well to prevent tip stall on the inner wing.

Fig. 26.3 (left) illustrates the system lift to drag ratio of differently sized pumping kite systems having identical aerodynamic characteristics in terms of glider lift and drag coefficients. Furthermore the tether length is identical for different sizes. Sizing of the tether thickness is based on the tension at a fixed airspeed and lift. In reality the tether length will grow slightly for increasing systems as will airspeed, which would have a softening effect on the differences in system lift to drag ratio. Fig. 26.3 (right) illustrates the glider and tether drag coefficients, which illustrates that the system lift to drag ratio grows for aerodynamically identical glider as the system is scaled up, thus tether drag is a bigger problem for smaller systems.

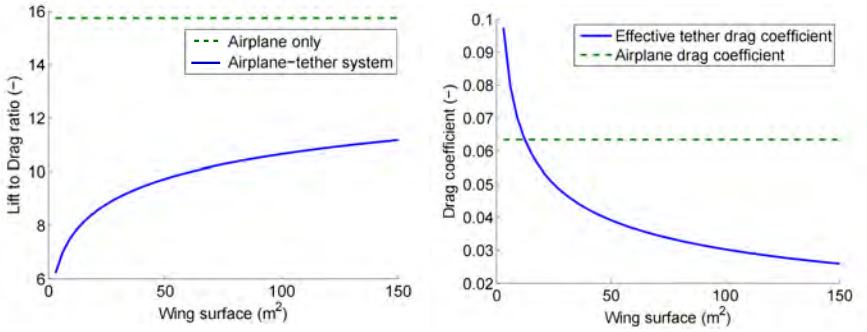


**Fig. 26.3** System lift to drag ratio (left) and total drag coefficient (right) as functions of glider wing surface area.

## 26.3 Guidance and Control

The simple analysis of airborne wind systems provided by Loyd in his 1980 paper [1] is based on equilibrium conditions and can be graphically defined by the force

and speed diagram as shown in Fig. 26.4. The definition of tether angles with respect to the wind direction is shown in Fig. 26.5.

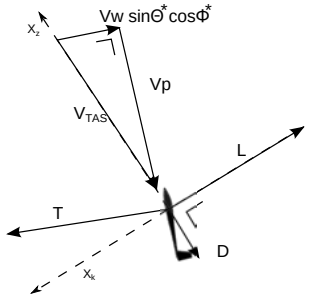


**Fig. 26.4** Force and speed diagram during power production for forces in equilibrium, showing identical ratios between $L/D$ and $V_p/V_w \sin\Theta^* \cos\Phi^*$. The dashed lines indicate the kinematic reference frame (x pointing in the direction of the airspeed).

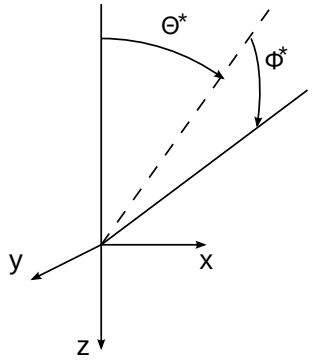


**Fig. 26.5** Definition of tether angles with respect to wind direction blowing along the x-axis. $\Theta^*$ is a negative rotation along the y-axis and $\Phi^*$ is a positive rotation along the x-axis.

The analysis of the equilibrium forces and velocities will over-estimate the total power production with respect to a real power cycle due to the assumption that the system is massless. In reality the glider is constantly maneuvering to stay inside the wind window and thus constantly accelerating hence not being in equilibrium. The true motion is governed by the equations of motion conventional to aircraft, Eqns. (26.1).

$$\begin{bmatrix} \dot{u} \\ \dot{v} \\ \dot{w} \end{bmatrix} = \frac{1}{m} \begin{bmatrix} X \\ Y \\ Z \end{bmatrix} + g \begin{bmatrix} -\sin\theta \\ \sin\phi\cos\theta \\ \cos\phi\cos\theta \end{bmatrix} - \begin{bmatrix} p \\ q \\ r \end{bmatrix} \times \begin{bmatrix} u \\ v \\ w \end{bmatrix} \tag{26.1a}$$

$$\begin{bmatrix} \dot{p} \\ \dot{q} \\ \dot{r} \end{bmatrix} = J^{-1} \left( \begin{bmatrix} L \\ M \\ N \end{bmatrix} - \begin{bmatrix} p \\ q \\ r \end{bmatrix} \times \left\{ J \begin{bmatrix} p \\ q \\ r \end{bmatrix} \right\} \right) \tag{26.1b}$$

$$\begin{bmatrix} \dot{\theta} \\ \dot{\phi} \\ \dot{\psi} \end{bmatrix} = \begin{bmatrix} 1 & \sin\phi\tan\theta & \cos\phi\tan\theta \\ 0 & \cos\phi & -\sin\phi \\ 0 & \frac{\sin\phi}{\cos\theta} & \frac{\cos\phi}{\cos\theta} \end{bmatrix} \begin{bmatrix} p \\ q \\ r \end{bmatrix} \tag{26.1c}$$

$$\begin{bmatrix} V_{\mathrm{N}} \\ V_{\mathrm{E}} \\ V_{\mathrm{D}} \end{bmatrix} = T_{\mathrm{nb}} \begin{bmatrix} u \\ v \\ w \end{bmatrix} + \begin{bmatrix} V_{\mathrm{wind_N}} \\ V_{\mathrm{wind_E}} \\ V_{\mathrm{wind_D}} \end{bmatrix} \tag{26.1d}$$

With $u$, $v$, $w$ velocity along respectively the body x, y, z axis, $p$, $q$, $r$ rotational rates along respectively the body x, y, z axis, $\phi$, $\theta$, $\psi$ the Euler angles, $V_{\mathrm{N}}$, $V_{\mathrm{E}}$, $V_{\mathrm{D}}$

velocity respectively north, east, down, $g$ the gravitational constant, $X$, $Y$, $Z$, aerodynamics and tether forces along respectively x, y, z axis, $L$, $M$, $N$ aerodynamic and tether moments around respectively the x, y and z axis and $T_{\mathrm{nb}}$ the transformation matrix from the body to the inertial reference frame, which can be found in any common book on aircraft dynamics.

The Loyd paper, [1] shows that the power the system delivers is proportional to $L^3/D^2$. Due to the large contribution of the tether drag to the total drag, AWE systems tend to fly at high L/D and pitching up counter-intuitively increases airspeed.

Compared to conventional glider flight, the flight maneuvers during the PowerPlane flight pattern may seem aggressive and nonlinear in the ground reference frame. However, when changing the control reference to a tether based reference frame, the same maneuvers become rather mild and practically speaking linear in the sense that dynamic coupling can be neglected and longitudinal and lateral control can be separated. The tether based 'Euler' angles then vary only up to $20^\circ$ for the roll and pitch angle.

The transformation from inertial reference frame to the tether based reference frame is defined by:

1. Rotation around the earth fixed z-axis by $\Psi$, the wind direction, with corresponding direction cosine matrix $T_{\mathrm{z}_{(\psi)}}$
2. Rotation around the y-axis by $-\Theta^*$, with corresponding direction cosine matrix $T_{\mathrm{y}_{(-\Theta^*)}}$
3. Rotation around the x-axis by $\Phi^*$, with corresponding direction cosine matrix $T_{\mathrm{x}_{(\Phi^*)}}$

$$C_{\mathrm{ti}} = T_{\mathrm{x}_{(\phi)}} T_{\mathrm{y}_{(-\theta)}} T_{\mathrm{z}_{(\psi)}} \tag{26.2}$$

With $C_{\mathrm{ti}}$ the direction cosine matrix mapping inertial coordinates into tethered coordinates and the other way around by taking the transpose, $C_{\mathrm{it}} = C_{\mathrm{ti}}^{\mathrm{T}}$. When introducing the conventional axis transformation from the inertial reference frame to the body fixed reference frame by means of the Euler angles (roll ($\phi$), pitch ($\theta$) and yaw ($\psi$)) as $C_{\mathrm{bi}}$, the direction cosine matrix to the body frame from the tethered frame is given by Eq. (26.3).

$$C_{\mathrm{bt}} = C_{\mathrm{bi}} C_{\mathrm{it}} \tag{26.3}$$

The tethered Euler angles are then derived consequently as in Eqns. (26.4).

$$\phi_{\mathrm{t}} = \tan^{-1}\left(C_{\mathrm{bt}_{(2,3)}} / C_{\mathrm{bt}_{(3,3)}}\right) \tag{26.4a}$$

$$\theta_{\mathrm{t}} = \sin^{-1}\left(-C_{\mathrm{bt}_{(1,3)}}\right) \tag{26.4b}$$

$$\psi_{\mathrm{t}} = \tan^{-1}\left(C_{\mathrm{bt}_{(1,2)}} / C_{\mathrm{bt}_{(1,1)}}\right) \tag{26.4c}$$

### *26.3.1 Longitudinal Control*

As can be concluded from the equations presented in Loyd [1] , the crux for high power outputs is flying at high system lift-to-drag ratios. Since the lift coefficient directly relates to angle of attack, this translates into a longitudinal control objective to track the angle of attack, which is actuated by the elevator surfaces. Angle of attack control alone is however not sufficient to control motion along the tether based z-axis.

Another important, but unconventional factor to the longitudinal control of the pumping kite system is the constraint imposed by the tether. The motion along the direction of the tether (heave) is defined by the rotational velocity of the winch, which thereby becomes a second longitudinal control input. It is important to view the control on the glider and the control of the winch as one.

Both control inputs affect the tether tension which can easily grow into instabilities. Lowering the angle of attack lowers the tension by lowering the lift generation of the wing, thereby also lowering the lift to drag ratio of the system (Fig. 26.2), which lowers the airspeed (which again lowers the tension). Raising the winch speed lowers the tension by lowering the airspeed. What makes this control problem more complicated is that communication between winch and glider is over radio suffering from transmission delays.

#### 26.3.1.1 Power Generation Phase

Due to communication latencies the longitudinal control uses the elevator passively (in a fixed position comparable to a flap) and the winch speed controls the tether tension. Note that this implies that the system does not operate at the optimal $V_w/3$ as derived by Loyd [1]. By fixing the elevator in effect the angle of attack and thus the lift coefficient is fixed. The tension demand is scheduled against airspeed such that at low airspeed the tension demand rises, while at high airspeed it drops.

Note that the winch control does depend on the glider measurement of the true airspeed. Compared to angle of attack changes, the airspeed however changes orders of magnitude slower since physically it is a derivative of higher or lower lift to drag ratio in tethered flight. Therefore the system latencies are acceptable in this control architecture.

#### 26.3.1.2 Reset Phase

As the tether length reaches its maximum the reset phase is triggered and activates a second set of longitudinal controls. In this setup the winch becomes the passive component by simply setting the winch speed to reeling in at maximum speed, thereby making the time for resetting the system as small as possible. The elevator is con-

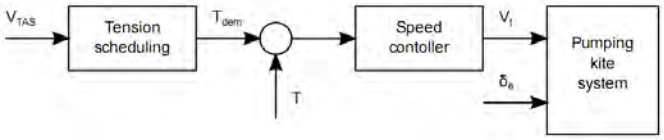


**Fig. 26.6** Block diagram indicating the functioning of the longitudinal control scheme during power generation.

trolled to maintain a specific flight path angle that is derived from a sink demand setting, which is scheduled against wind speed. The transition from the power production phase into the reset phase is driven by the acceleration limit of the winch (5 $m/s^2$) and takes up to 4 seconds in extreme conditions. During the reset phase the winch always achieves the maximum reel speed regardless of the wind speed.Since the winch speed in this phase is set, so is the ground speed. Which implies that the true airspeed, and thus the drag, rises with increasing wind. The scheduling is selected to have the reset phase consist of a steeper dive for higher wind speeds such that gravity compensates for the glider drag as much as possible, yet never makes it exceed the tether speed.

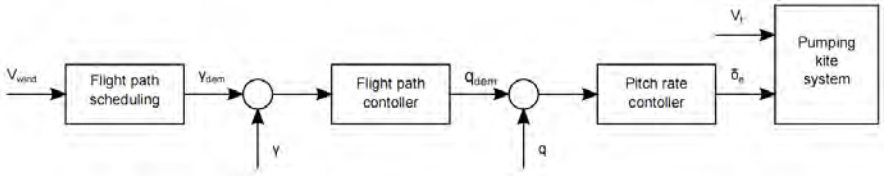


**Fig. 26.7** Block diagram indicating the functioning of the longitudinal control scheme during system reset.

### 26.3.1.3 Phase Transitions

The change between control strategies is instant and the plane enters the reset phase with a fast pitch down maneuver. The tether tension is suddenly lowered and the tether may go slack for a brief period. Shortly after the winch will however pick up the pace and straighten out the tether.

During the transition back into the power generation flight path the plane is flying into the wind at ground speeds roughly equal to the winch speed, such that the effective wind speed is that of the true wind plus that of the tether. The tether tension is low and approximately a full order of magnitude lower than during power generation. If the winch response is too slow this would cause a high airspeed. On the other hand if the winch responds too fast, the tension will drop completely and the plane would not make the turn back into the pattern at all, or it would build up momentum and at some point instantly tense the tether resulting in high shock loads. In other

words the tether may not get slack, but it can also not build up tension, making the transition back into the pattern a delicate maneuver.

This creates hard requirements on the synchronization, making the radio latencies unacceptable. For 'communication' in this situation the tether tension is used. This method, in combination with the fixed elevator, has proven to be fast and provides sufficient margin for different wind speeds.

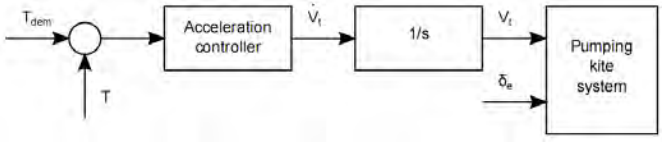


**Fig. 26.8** Block diagram indicating the functioning of the longitudinal control scheme during transition into the power generation phase.

### *26.3.2 Lateral Control*

Essentially the lateral control is not much different from a conventional glider. The main difference compared to a free flying glider is that the lateral control is not defined with respect to the inertial reference frame, but with respect to the tether frame as defined in the beginning of this section.

The flight path is defined by waypoints in the spherical tether coordinates, Fig. 26.5, making the waypoints independent of tether length and wind direction. For flight guidance these spherical coordinates are mapped into the tether reference frame, with the origin in the generator, thereby generating waypoints in Cartesian coordinates. The tether coordinates of the flight path thereby do depend on wind direction and tether length ($R$), Eq. (26.5).

$$\begin{bmatrix} x \\ y \\ z \end{bmatrix}_{\mathrm{i}} = C_{\mathrm{it}} \begin{bmatrix} 0 \\ 0 \\ R \end{bmatrix}_{\mathrm{t}} \tag{26.5}$$

As opposed to the longitudinal control, only one controller governs the actual waypoint tracking. The lateral controller derives the closest point on the set flight path from its current position. A variable look ahead distance (scheduled vs. tether length) is mapped on the flight path to determine a so called look ahead point. The direction toward this look ahead point is the track demand. A controller transforms the track error into a roll angle reference and this error is mapped into a roll rate, Fig. 26.9.

During power generation the flight path is a lemniscate, or lying figure of eight (see Fig. 26.10). During the system reset it is a straight line starting at the loca-

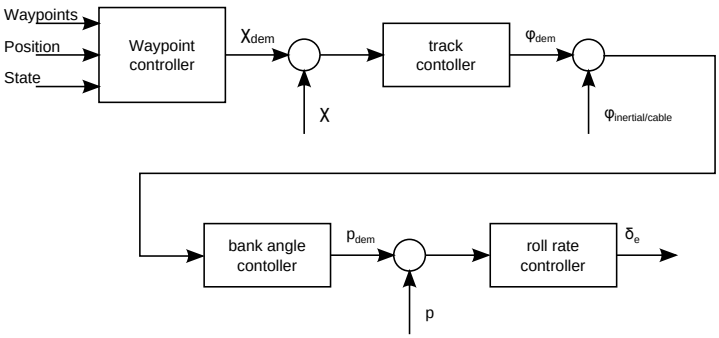


**Fig. 26.9** Block diagram indicating the functioning of the lateral control scheme.

tion where the corresponding phase was activated and ending in the coordinates of pattern reentry.

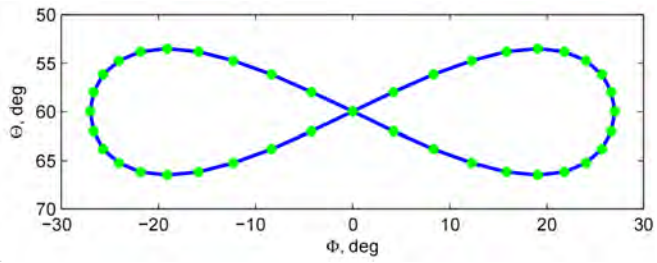


**Fig. 26.10** Scheduled waypoints during the power generation phase in tether angles

### *26.3.3 State Machine*

The flight paths between the crosswind pattern and the system reset phases are quite different and a higher level state-selector is implemented to switch between phase specific controllers. This state machine determines which controllers are active and resets the integrators of inactive controllers.

Each state has a predefined set of criteria (flags, demands) that must be met to transition into a next state. Depending on the state, one or several transitions are possible. Furthermore in each state an abort can be triggered when exceeding the margins to the flight envelope, which triggers a completely independent control system with its own state machine and consequent states and controllers to take over. Table 26.1 presents an overview of the relevant states for power generation.

**Table 26.1** Pumping kite states used in power generation and corresponding criteria to complete the task of that state and trigger transition into a next state

| State | Condition | Next state |
|---|---|---|
| Takeoff | Completed when reaching a set altitude and climb rate | Climb |
| Climb | Completed when reaching a set altitude | Pattern entry |
| Pattern entry | Completed when within a set range to the pattern | Power generation |
| Power generation | Completed when reaching a dynamically set tether length | Pattern exit |
| Pattern exit | Completed when reaching a set waypoint | Reset |
| Reset | Completed when reaching a minimum tether length | Pattern re-entry |
| Pattern re-entry | Completed when within a set range to the pattern | Power generation |

## 26.4 Flight Performance of the Control System in Test Flights

The performance of the pumping kite system is illustrated by Figs. 26.11 and 26.12 that present one complete power cycle starting in a reset phase, followed by a complete power generation phase and ends in the middle of another reset phase. The tether tension and speed, the true airspeed and angle of attack, Euler angles and tether based position and attitude are presented.

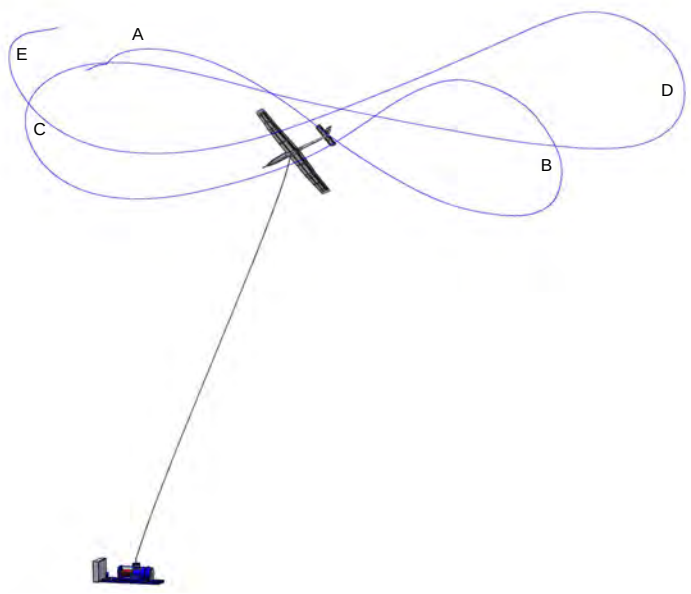


**Fig. 26.11** A 3D representation of the flight pattern. The performance of the system during this pattern is shown in Fig. 26.12 and is mapped onto the flight path through the letters A–E.

Comparing tethered Euler angles to the conventional ones illustrates the linearizing effect mentioned in Sect. 26.3. The tethered pitch angle varies approximately $20^\circ$ from $-20^\circ$ to $0^\circ$ and the tethered roll angle varies within $-10^\circ$ to $30^\circ$. The large negative pitch angle that is observed is due to the system being reset, where the plane flies toward the winch. With the tether being much longer than the flight altitude, this results in large negative pitch angles.

The angle of attack is tracked satisfactory in the beginning (to within plus or minus $1^\circ$). In the middle some oscillations are observed that however dampen out toward the end of the phase. Note that the oscillations in angle of attack have a strong correlation to the tether tension, but much less to the glider airspeed.

The path tracking may seem poor when looking at the waypoint pattern and the actual flight path. Note however that the path that is being tracked is defined by the look-ahead point as it shifts over the waypoint pattern and as such the pattern itself has only a loose relation to the flight path that is tracked. When multiple power loops are compared, the flight paths overlap which is a better indication of the tracking performance.

The control scheme that is presented here works quite well when tuned properly. In order to prevent the aircraft from entering into an unrecoverable state, there is another layer of checks that is applied on top of the control system. The aircraft states are checked against preset boundary conditions. When one of the boundary conditions is met, the aircraft cuts the tether and enters a free-flight mode where the wing is leveled and the airspeed controlled to the free flying airspeed demand. In order to further mitigate the risk of crashing the aircraft, it is steered into a circular pattern around the ground winch such that the human pilot can take control of the aircraft while the aircraft is in stable flight.

## 26.5 Conclusions

Through choosing the tether based reference frame and carefully selecting control variables, simple control schemes are well capable of flying the highly aggressive patterns of the pumping kite system. In lateral direction the glider is controlled by means of a waypoint controller that produces track demands. Tracking errors generate roll angle demands, which again are used to create roll rate demands each through linear controllers. The longitudinal motion is controlled by fixing the elevator and thereby fixing the lift coefficient and system lift to drag ratio in combination with a tension controller determining the tether velocity. The actual angle of attack varies with $\pm$ 1.5 $^\circ$ during the power production phase.

The result of flight tests show that the controllers are sufficiently robust to track a power cycle that is independent of airspeed and direction over a wide range of wind speeds. The actual power produced during these flight tests is limited by a large number of system specific factors such as maximum tether tension, maximum loads on the aircraft etc. but also due to constraints in efficiency of the grid connection systems. To allow benchmarking between different configurations we use only the

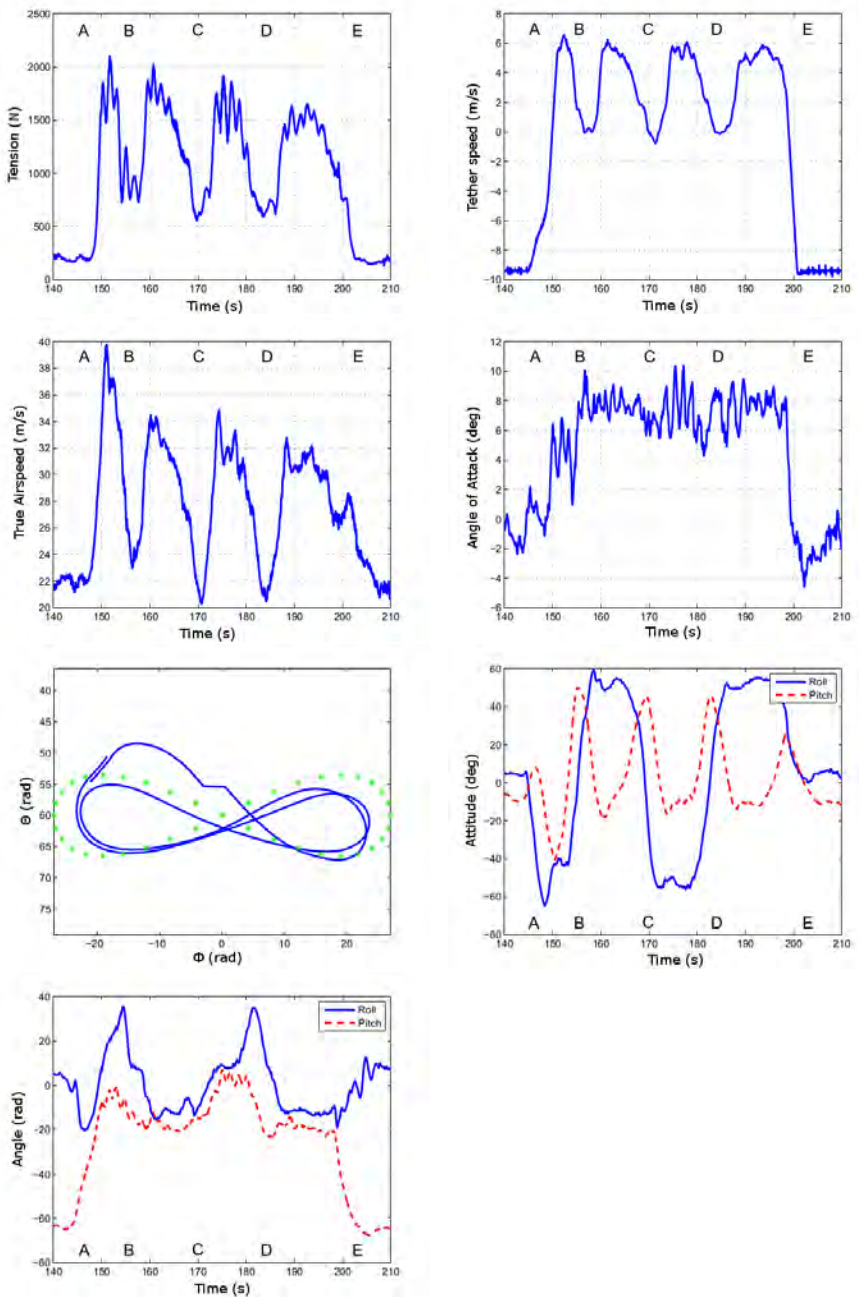


**Fig. 26.12** Test results of one power cycle at 7 m/s wind speed, measured at 6.5 m reference height. Starting point of the graphs is the reset phase, followed by power generation and ending in another reset phase.

mechanical power that is delivered to the generator and electronic back-end. Thus, in this section we will only present the power that is delivered to the generator by means of the product of tether tension and tether velocity (or the product of torque on the generator shaft and the angular velocity of the shaft). The electrical power that is delivered back to the power grid is typically about 50 % of these values in the current system.

Fig. 26.13 shows a typical power curve as function of time for a full power cycle. The curve is normalized to the total cycle time and is taken at approximately 9 m/s wind speed. The curve clearly shows the effect of gravity on the power production. Note that the current flight pattern (i.e. the lemniscate) is a non-optimized pattern that is only selected as base line for the control development. Once more optimal patterns will be flown we expect that the difference between the maximum and minimum power over one pattern will come closer together towards the average. Also, the current pattern is defined by a rise angle of $30^\circ$ with the horizon and a bank angle of $30^\circ$ with the wind direction. A smaller pattern flown closer to the ground (i.e. $20^\circ$) will improve the power differences over one pattern and thus over the full power production cycle.

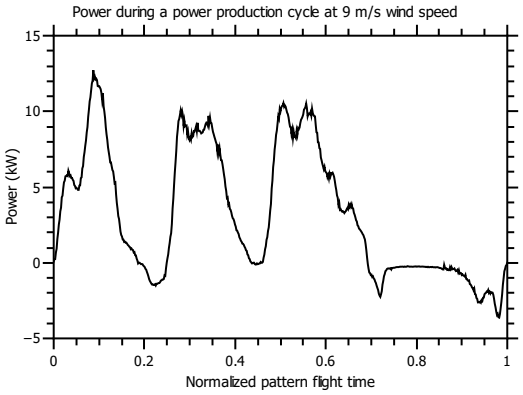


**Fig. 26.13** Instantaneous traction power during one full cycle at 9 m/s wind speed, normalized to the cycle time

One of the development targets for 2013 is to produce a first power curve of the PowerPlane system. With the limited data set that is available at this time and the intrinsic system limitations there is insufficient data to fully define the power curve. Yet it is interesting to look at the preliminary power curve as depicted in Fig. 26.14 to indicate the effects of these limitations on the shape of the curve.

Although we know that the actual performance of the systems in terms of the power output can be greatly improved by changing the rise- and wind direction angles, aircraft strength, winch speed etc. it is interesting to see what the power factor $\zeta$ of the system would be at this moment. This value is defined in Eq. (1.10) of Chap. 1 to compare the output of an AWE system to the wind power density of a surface are with the same cross sectional surface area as the wing surface area of the AWE system (i.e. 3 $m^2$ for the current prototype). Fig. 26.15 shows the value of $\zeta$ as a function of wind speed. The figure clearly indicates the effect of the limitations of

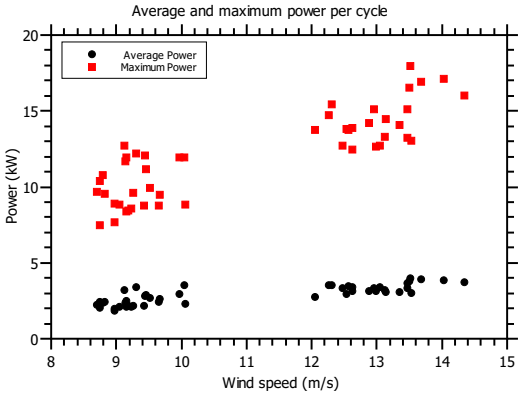


**Fig. 26.14** Preliminary power curve for the current PowerPlane prototype. The power levels for higher wind speeds are limited by the system constraints such as maximum lift force that the aircraft can sustain.

the generator and aircraft strength which are primarily a consequence of the focus on control development and not system performance. Given the theoretical maximum of $\zeta$=30 for a lift coefficient $c_l$=1 the current system is far from optimum. The tether tension is maximized in the control loop by the winch speed control. Therefore, at higher wind speeds, the fraction of the wind power density that is converted into electrical power is much smaller than at lower wind speeds. This causes a much smaller $\zeta$ value at higher wind speeds. Ampyx Power aims at optimizing the current 3m$^2$ wing and ground station to fully determine the power curve and maximize the value of $\zeta$ over the full operational envelope in the 2013 flight campaign.

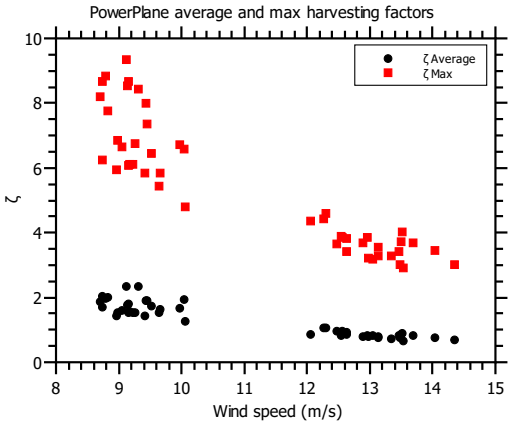


**Fig. 26.15** Harvesting factor for the current PowerPlane prototype. The average harvesting factor ($\zeta$) is given together with the peak harvesting factor.

ζ Average
ζ Max

## References

1. Loyd, M. L.: Crosswind kite power. Journal of Energy **4**(3), 106–111 (1980). doi: 10.2514/3.48021
2. Sieberling, S.: Flight Guidance and Control of a Tethered Glider in an Airborne Wind Energy Application. In: Chu, Q., Mulder, B., Choukroun, D., Kampen, E.-J., Visser, C., Looye, G. (eds.) Advances in Aerospace Guidance, Navigation and Control, pp. 337–351. Springer, Berlin-Heidelberg (2013). doi: 10.1007/978-3-642-38253-6_21
3. Sieberling, S., Ruiterkamp, R.: The PowerPlane an Airborne Wind Energy System. AIAA Paper 2011-6909. In: Proceedings of the 11th AIAA Aviation Technology, Integration, and Operations (ATIO) Conference, Virginia Beach, VA, USA, 20–22 Sept 2011. doi: 10.2514/6.2011-6909